IJEAS
International Journal of Energy and Applied Sciences

Effect of Hvof Process Parameters on The Tribological Performance of $Al_{65}Cu_{20}Fe_{15}$ Coatings on Aisi 321 Substrate

Dilnoza Baltabayeva[1], Sherzod Kurbanbekov[2] , Sattar Bekbaev[2], Aidyn Tusupzhanov[3], Ali Choruh[4], Berik Kaldar[2*]

[1] D. Serikbayev East Kazakhstan Technical University, Ust-Kamenogorsk, Kazakhstan, dilnoza.baltabayeva@ayu.edu.kz
[2] Kh. A. Yassawi International Kazakh-Turkish University, Turkestan, Kazakhstan, sherzod.kurbanbekov@ayu.edu.kz, sattarbek.bekbayev@ayu.edu.kz,
[3] Nazarbayev Intellectual School of Chemistry and Biology, Turkestan, Kazakhstan, tussupzhanov_a@trk.nis.edu.kz
[4] Sakarya University, Sakarya, Turkey, coruh@sakarya.edu.tr
Correspondence: berik.kaldar@ayu.edu.kz

Received: 1 April 2026
Revised: 22 April 2026
Accepted: 4 May 2026
Published: 25 May 2026

https://doi.org/10.47526/2026-1/2505-3123.01.

Abstract

This study systematically investigates the influence of high-velocity oxygen-fuel spraying (HVOF) parameters, with a particular emphasis on oxygen pressure, on the microstructure and tribological performance of $Al_{65}Cu_{20}Fe_{15}$ coatings. The coatings were deposited at two oxygen pressures (3.0 and 3.5 bar) while maintaining other spraying process parameters constant. Microstructural characterization was performed using scanning electron microscopy (SEM) and energy-dispersive spectroscopy (EDS), and the phase composition was analyzed to assess the proportion of quasi-crystalline and crystalline phases. Tribological behavior was evaluated using a ball-on-disk sliding friction test with continuous recording of the friction coefficient. The results show that oxygen pressure significantly affects the coating density, phase composition, and tribofilm formation. The coating applied by spraying at 3.5 bar demonstrated the most balanced performance, with a stable friction coefficient of 0.55-0.60 and consistent wear, due to a higher proportion of the quasi-crystalline phase and a homogeneous tribofilm. Thus, the analysis revealed that processing the samples at 3.5 bar oxygen pressure is the optimal process mode, ensuring the formation of a dense microstructure and improved tribological properties of the coating.

Keywords: Al-Cu-Fe; HVOF; tribology; XRD, SEM; friction coefficient; EDS.

1. Introduction

Modern materials science places particular emphasis on the development of wear-resistant and corrosion-resistant coatings designed for use in extreme conditions - high temperatures, abrasive loads, and exposure to aggressive environments. Therefore, one of the pressing challenges is increasing the durability and reliability of structural materials used in the aerospace, energy, and mechanical engineering industries [1]. To address this challenge, coatings produced by rapid crystallization methods are increasingly being used. These methods allow the formation of microstructures with a unique combination of crystalline, amorphous, and quasi-crystalline phases [2]. Quasi-crystalline materials with quasi-periodic atomic order possess a combination of exceptional properties: high hardness, low friction coefficient, excellent corrosion resistance, and stability at temperatures up to 800 °C [3]. Among the various quasi-crystal-forming alloys, the Al-Cu-Fe system is of particular interest , in particular the $Al_{65}Cu_{20}Fe_{15}$ alloy , which forms a stable quasi-crystalline phase [4].

Coatings based on this alloy are characterized by microhardness in the range of 700-1500 HV , a low coefficient of friction (up to 0.1 under dry friction) and high adhesion, which makes them promising for protecting working surfaces under conditions of intense wear [5].

HVOF spraying is the most effective [6]. It combines high particle velocity (up to 700 m/s) and relatively low substrate temperature (100-200 °C), minimizing thermal stress and preserving the original phase structure of the alloy. High kinetic energy and limited contact of particles with oxygen ensure minimal oxidation and high coating density [6].

The substrate used in this study was 08Kh18Ni10T (AISI 321) stainless steel, which is widely used in industry due to its combination of high corrosion resistance, heat resistance, and ductility. The steel contains approximately 18% chromium, 10% nickel, and titanium as a stabilizing element that prevents intergranular corrosion. AISI 321 steel has a tensile strength of 530–730 MPa, a yield strength of 200–250 MPa, a relative elongation of 40–50%, a hardness of ≈180 HV, and maintains structural stability at temperatures up to 800 °C [7]. Due to these properties, AISI 321 steel is widely used in the chemical, oil and gas, food, and power industries, especially for the production of pipelines, heat exchangers, reactors, pressure vessels, and turbine components.

Despite their inherent strength, even stainless steels can be damaged by friction, erosion, and extreme temperatures. To combat this, the application of quasi-crystalline Al-Cu-Fe coatings has proven to be a highly effective way to extend the service life of these steels. These coatings achieve this by reducing friction and improving protection against oxidation and wear.

2. Materials and Methods

AISI 321 austenitic stainless steel (15×45×3 mm³), designed for machining and thermal spraying, was used as the substrate. This steel is alloyed with titanium, which increases its resistance to intergranular corrosion and thermal aging. Before coating application, the substrate was sandblasted with white corundum to increase surface roughness and improve coating adhesion (Table 1).

Table 1. Chemical composition of AISI 321.

C	Mn	P	S	Si	Cr	Ni	Ti	Fe
0.08	2.0	0.045	0.03	1.0	17.0-19.0	9.0-12.0	0.5	Rest

Aluminum (Al), copper (Cu), and iron (Fe) powders were provided by Hebei Suoyi New Material Technology Co., Ltd. (Handan, China) with a purity greater than 99.5%. The surface morphology of the Al-Cu-Fe powders is shown in Figure 1. The particles have an irregular polyhedral shape, combining angular and plate-like elements, which is typical of materials obtained by mechanical alloying. This morphology typically results in lower flowability compared to spherical powders, but provides a large surface area favorable for coating adhesion during thermal spraying.

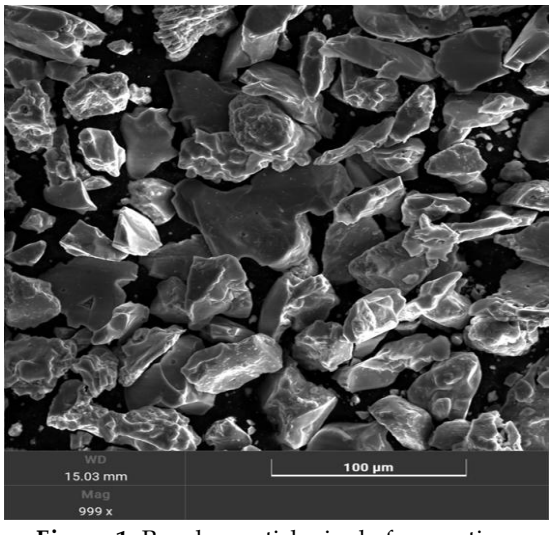

Figure 1. Powder particle size before coating.

Particle size analysis revealed a wide range, from 10 to 80 μm, specifically, the 10th percentile was 18 μm, the median (50th %) was 40 μm, and the 90th % was 75 μm. This particle size profile is beneficial for smooth processing and stable material feed in HVOF technology [8,9].

The observed cubic crystal structure, along with minor shifts in the diffraction peaks, indicates the presence of both quasi-crystalline and crystalline regions in the synthesized powder. This dual nature contributes to a favorable balance of hardness, oxidation resistance, and low friction. Therefore, the $Al_{65}Cu_{20}Fe_{15}$ composition is promising for the development of coatings capable of withstanding high temperatures and wear [9].

This study focuses on the impact of oxygen pressure during the HVOF spraying process. This specific parameter is critical for controlling particle velocity, temperature distribution, and the degree of oxidation during coating formation. To ensure reliability and consistency of the results, each experiment was repeated three times. Oxygen pressure directly affects the velocity and turbulence of the gas flow. This, in turn, affects how well the particles melt, the energy of their impact on the substrate, and ultimately the microstructure, density, and adhesion of the coating [10].

This experimental strategy is based on the methodologies developed by Huttunen-Saarivirta et al. and Wolf et al. Their work showed that by holding all variables constant except the one under study, stable thermal and kinetic conditions are achieved. This stability is necessary for accurately understanding the influence of a single factor on the coating properties [11,12]. Spray parameters were selected based on the performance characteristics of the HVOF process described in [25] and the key requirements for producing high-quality coatings. A spray distance of 250 mm between the nozzle and the substrate was chosen to ensure an optimal balance between particle temperature and impact velocity, preventing excessive overheating and preserving the integrity of the quasi-crystalline structure. A propane pressure of 1.9 bar was used to maintain stable combustion, ensuring uniform heating of the powder particles without complete melting. Oxygen pressure varied between 3.0 and 3.5 bar to optimize particle kinetic energy, increase coating density, and enhance adhesion strength. An air pressure of 2.2 bar ensured complete combustion of the propellant, effectively reducing the risk of particle oxidation during flight to the substrate (Table 2).

The selected parameters resulted in stable combustion, uniform spray pattern, and high-quality coating. Thanks to the optimal particle size and appropriate spray distance, the powder spent sufficient time in the flame for effective heating and reached the substrate with the required energy, as evidenced by the uniform and homogeneous nature of the deposited layer. Maintaining the quasi-crystalline structure was key throughout the process. A controlled environment ensured that the unique properties of the $Al_{65}Cu_{20}Fe_{15}$ alloy were preserved in the final coating. The interaction between particle characteristics, spray parameters, and the resulting coating microstructure was thoroughly investigated, with particular emphasis on the role of oxygen pressure in achieving the desired performance characteristics. Consistent and reproducible results obtained in triplicate experiments underscore the robustness of the chosen methodology and the validity of the conclusions regarding the effect of oxygen pressure on the HVOF coating process. This systematic approach enables precise understanding of how to optimize coating properties for challenging high-temperature, wear-resistant applications.

Table 2. HVOF parameters

№	Propane (bar)	Oxygen (bar)	Air (bar)	Distance (mm)
Sample A	1.9	3.0	2.2	250
Sample B	1.9	3.5	2.2	250

The phase composition of the applied coatings was analyzed by X-ray diffraction (XRD) using a Panalytical X'Pert PRO diffractometer (Philips, Amsterdam, the Netherlands) equipped with a copper anode generating Kα radiation (λ = 1.5406 Å). All measurements were performed at room temperature (25°C) at an operating voltage of 40 kV and a current of 30 mA. Diffraction patterns were recorded in the 2θ range from 20.01° to 89.99° with a step size of 0.02° and a counting time of 2 sec per step. Phase identification and analysis were performed using the HighScore Plus software package.

The surface morphology and elemental composition of the coatings were examined by scanning electron microscopy (SEM) using a Tescan Vega 4 microscope (Brno, Czech Republic). Tribological performance was assessed using sliding wear tests conducted on a TRB3 tribometer (Anton Paar, Buchs, Switzerland) in a ball-on-

disk configuration. The tests were conducted under dry sliding conditions with a normal load of 2 N, a sliding velocity of 1 cm/s, and a total sliding length of 30 m. A 100Cr6 steel ball with a diameter of 6 mm was used as the counterball. The wear rate of both the coating and the counterball was determined according to ASTM G99.

Microhardness measurements were performed using the Vickers indentation method in accordance with ASTM E384 using an HLV-1DT microhardness tester. A diamond pyramidal indenter with an apex angle of 136° was applied under a load of 0.5 kgf (4.9 N) for 10 s ($HV_{0.5}$). Hardness values were calculated based on the measured lengths of the two diagonals of the indentation (d_1 and d_2).

3. Results and Discussion

X-ray diffraction analysis revealed the presence of $Al_{0.5}Fe_{1.5}$ and $Al_{78}Cu_{48}Fe_{14}$ phases in samples coated with a quasicrystalline layer deposited by the HVOF method using propane, oxygen, and air. An examination of the diffraction patterns (Figure 2) indicates a clear correlation between the deposition parameters and the phase composition: with varying deposition conditions, the intensity of the diffraction peaks corresponding to the $Al_{0.5}Fe_{1.5}$ phase decreases, while those associated with the quasicrystalline (QC) phase become more pronounced. Quasicrystals are inherently complex materials characterized by a lack of translational symmetry and a virtually infinite unit cell. Structurally similar, but fully crystalline, approximant phases (AP) [14] are considered less complex than QC phases [25]. The intermetallic compound $Al_{0.5}Fe_{1.5}$, a well-ordered solid phase in the Fe-Al system, contains approximately 25 atomic percent aluminum. Under ambient conditions, this compound crystallizes in the cubic space group Im-3m with a unit cell parameter of approximately a = 2.91 Å [15]. The DO_3 arrangement of Fe and Al atoms in this structure increases the hardness and stability of the material compared to conventional Fe-Al solid solutions. In terms of tribological performance, $Al_{0.5}Fe_{1.5}$ coatings deposited by the HVOF method exhibit a relatively high friction coefficient ($\mu \approx 0.6$-0.7) during dry sliding on hard substrates such as steel [16]. This increased friction is mainly attributed to the metallic nature of the intermetallic compound and adhesive interactions at the contact surface. Wear analysis shows that $Al_{0.5}Fe_{1.5}$ coatings are predominantly subject to adhesive-abrasive wear, leading to the formation of microcracks. Despite its increased hardness, the intermetallic compound exhibits moderate brittleness, which contributes to the formation of cracks and chips under mechanical loads.

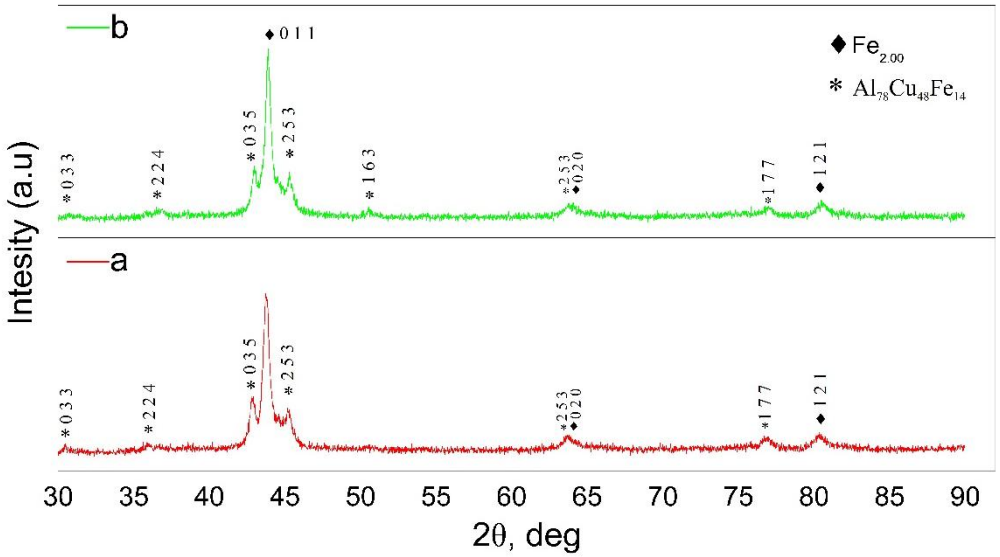

Figure 2. X-ray diffraction analysis.

In coatings obtained by the HVOF method, the quasicrystalline structure can be formed either directly from the original powder, which is pre-crystallized into a quasicrystalline state by rapid cooling of the melt, or in situ during high-speed sputtering and subsequent rapid solidification of the particles upon impact with the substrate. In the studied Al-Cu-Fe coatings with a composition in the range of $Al_{62\text{-}63}Cu_{20\text{-}25}Fe_{12\text{-}15}$, the predominant phase is the icosahedral quasicrystalline phase [17]. The identified $Al_{78}Cu_{48}Fe_{14}$ phase has a cubic crystalline structure with the space group Pm-3 and the unit cell parameter a = 12.3120 Å, reflecting the complex

atomic arrangement characteristic of ordered intermetallic compounds in the Al-Cu-Fe system. The presence of such a phase contributes to an increase in the hardness and structural stability of the coating due to the dense atomic packing and strong interatomic interactions within the lattice. One of the most notable features of the quasicrystalline phases of Al-Cu-Fe is their high hardness. The literature indicates that the microhardness of the icosahedral quasicrystalline phase in Al-Cu-Fe can reach approximately 10 GPa [18], which corresponds to approximately 1000 HV on the Vickers scale. Experimental measurements show that the microhardness of Al-Cu-Fe coatings deposited by HVOF spraying exceeds that of the widely used 6061-T6 aluminum alloy by 4-6 times [19]. It has been shown that the main properties of these coatings are highly dependent on their phase composition. The degree of quasi-crystallinity in sprayed coatings depends on deposition conditions, which affect the stability region of the quasicrystalline phase in the Al-Cu-Fe phase diagram as a function of temperature [20]. Coatings with higher aluminum and lower iron contents exhibit different stages of development of the final stable structure. With increasing temperature, their diffraction patterns indicate a phase transition from an icosahedral quasicrystalline phase to a crystalline approximant [21].

The polyhedral morphology of Al-Cu-Fe powder, which combines angular and plate-like shapes, can significantly impact the HVOF spraying process. First, this particle geometry can reduce powder flowability, which in turn can lead to uneven powder feed into the HVOF gun and promote agglomeration [25]. This can lead to instability in the spraying process, especially in systems using propane as a fuel, where stable combustion and uniform particle acceleration are highly dependent on uniform powder injection. Second, the complex particle shape can lead to uneven heating during flight. An increase in the specific surface area of fragmented Al-Cu-Fe particles increases their susceptibility to oxidation, especially at elevated oxygen pressure. Third, irregular morphology can affect coating formation: sharp edges can improve mechanical adhesion to the substrate, but can also result in a rougher surface topography and promote the formation of localized defects such as microcracks or unmelted particle residues.

In this study, two combustion modes were considered using propane at a constant pressure of 1.9 bar, with oxygen pressures varying to 3.0 and 3.5 bar. The air pressure was maintained at 2.2 bar, and the spray distance was 250 mm. The HVOF process is characterized by short particle residence times in the flame and the limited thermal conductivity of Al-Cu-Fe alloys. As a result, larger or irregularly shaped particles may not reach full thermal equilibrium in flight, which reduces their deformability upon impact with the substrate and contributes to the formation of microstructural heterogeneity in the coating.

Figure 3 shows the dependence of the friction coefficient on the sliding distance. 100Cr6 steel, a standard bearing material, was used as the counterweight, ensuring the practical relevance of the results. Increasing the oxygen pressure from 3.0 to 3.5 bar promotes more complete heating of the particles, improves their plastic deformation, and forms a denser and more uniform coating microstructure.

Tribological tests (5 N, 5 cm/s, 90 m) showed that sample B (3.5 bar) exhibited superior wear resistance: the wear area was 5764.3 μm^2, and the wear rate was $2.414 \cdot 10^{-4}$ mm^3/N m. For sample A (3.0 bar), these values were 11,987.6 μm^3 and $5.021 \cdot 10^{-4}$ mm^3/N m, respectively. Thus, an oxygen pressure of 3.5 bar ensures optimal tribological properties of the Al-Cu-Fe coatings.

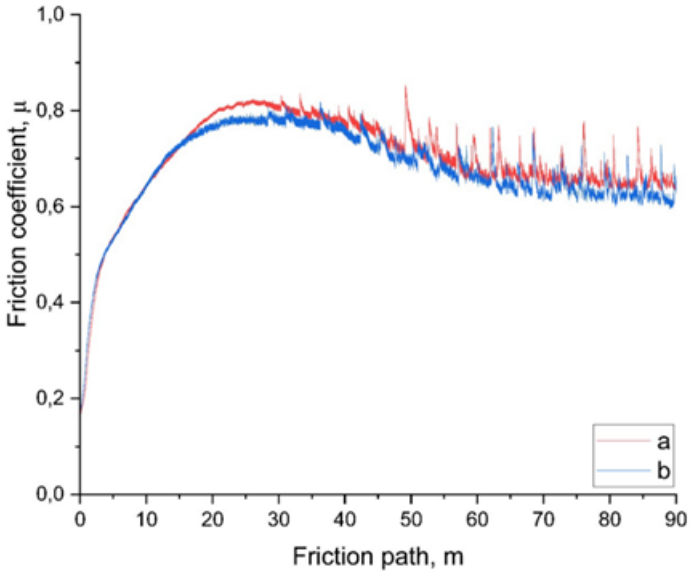

Figure 3. Friction coefficient versus friction path.

The friction curves (Fig. 3) reflect differences in the tribological behavior of the samples. Sample A (3.0 bar O_2) is characterized by a smooth running-in phase and a steady-state friction coefficient of 0.70-0.72 ± 0.02. The small oscillation amplitude indicates the formation of a stable friction film. The increased friction is due to the predominance of the intermetallic Fe_2Al ($Al_{0.5}Fe_{1.5}$) phase, which forms a more metallic contact layer and enhances adhesion to the 100Cr6 counterface.

Sample B (3.5 bar O_2) demonstrates a decrease in the friction coefficient to 0.55-0.60 ± 0.05 with a more stable curve. The improved performance is due to the increased proportion of the quasi-crystalline Al-Cu-Fe phase and a more homogeneous microstructure. Low surface energy and limited dislocation mobility of quasicrystals contribute to reduced adhesion and the formation of a stable slip film [25]. Furthermore, optimal thermal treatment increases coating density and reduces the number of wear-initiating defects.

A clearly defined interface is observed at the interface between the coating and the steel substrate (Figure 4). The coating thickness varied from 40.87 to 115.41 μm and was 43.97 ± 3.0 μm for sample A and 101.89 ± 13.5 μm for sample B. No signs of chemical interaction or the formation of intermetallic phases at the interface were detected, indicating a predominantly mechanical adhesion. This adhesion is due to the high kinetic energy of the particles during spraying and the developed roughness of the substrate surface after sandblasting.

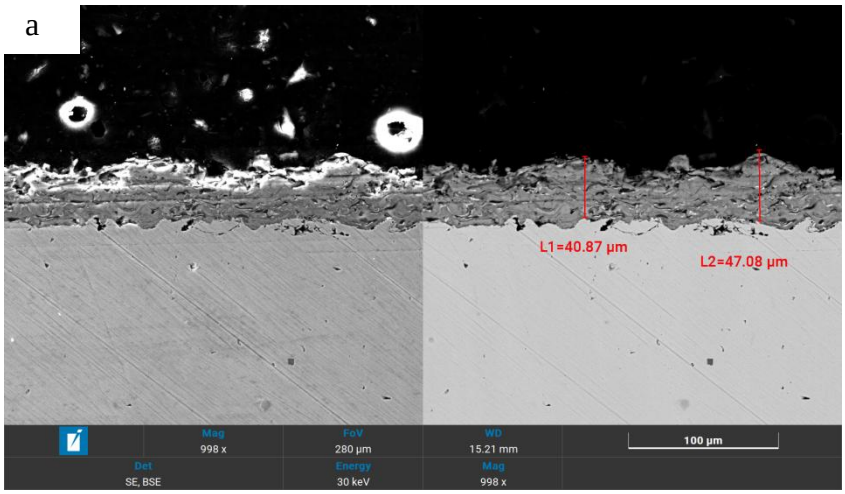

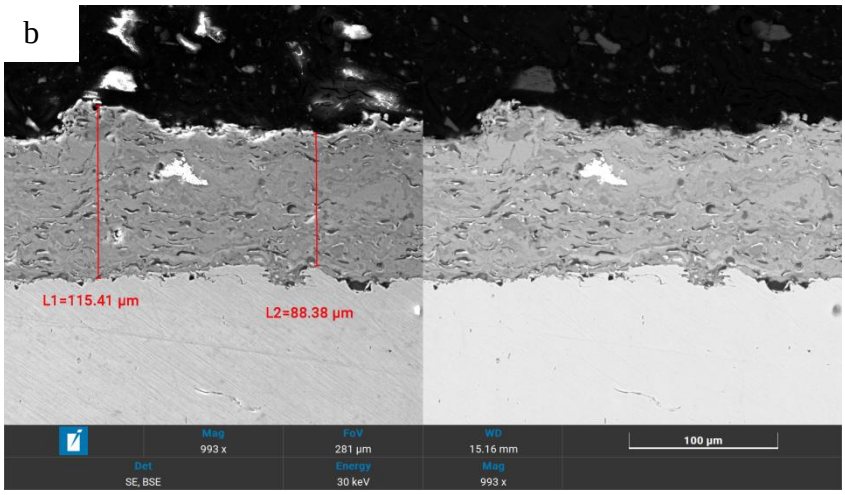

Figure 4. Thickness micrographs of Al-Cu-Fe coatings. Samples (a-b).

Furthermore, SEM micrographs of wear scars are shown in Figure 5. Analysis of the wear zone morphology revealed significant differences in scar width between samples (a-b), reflecting variations in wear mechanisms and material removal rates. The measured wear scar widths for the three coatings ranged from approximately 640 to 745.41 µm, indicating that surface degradation was primarily driven by abrasive wear, as evidenced by the presence of distinct parallel striations. The calculated wear index (WI) for the coatings ranged from 0.0002414 to 0.0005368 mm^3/Nm, with a larger wear scar area corresponding to reduced wear resistance, as expected. SEM observations revealed that sample A, which exhibited the lowest friction, had the narrowest wear scar among the three coatings. In this wear zone, the surface was relatively smooth and partially covered by a thin tribofilm formed during sliding. The absence of extensive delamination or cracking suggests that the dominant wear mechanism was gradual abrasive removal of the surface layer, facilitated by the formation of a stabilizing tribolayer. This behavior is consistent with the lower friction values recorded during tribological testing.

In contrast, sample B, characterized by the highest friction coefficient and pronounced fluctuations, exhibited a significantly wider wear band. Scanning electron microscope images revealed more intense material removal, accompanied by localized microcracks and partial delamination of the lamellae. These features indicate a decrease in wear resistance and a wear mechanism dominated by a combination of abrasive wear and microcrack propagation.

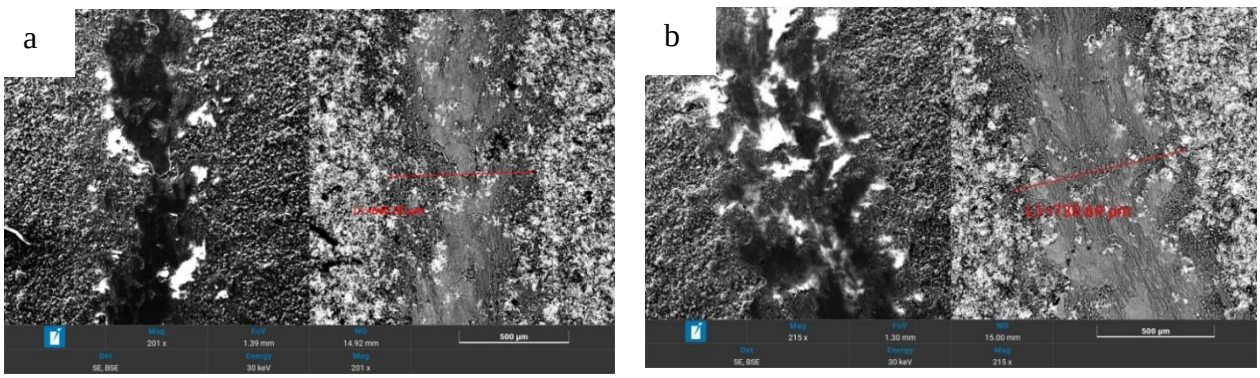

Figure 5. Micrographs of wear traces on Al-Cu-Fe coatings.

Figures 6, obtained in secondary electron (SE) and backscattered electron (BSE) modes, show characteristic areas of the coatings of samples a and b (oxygen pressure 3.0 bar and 3.5 bar), selected for local and linear EDS analysis.

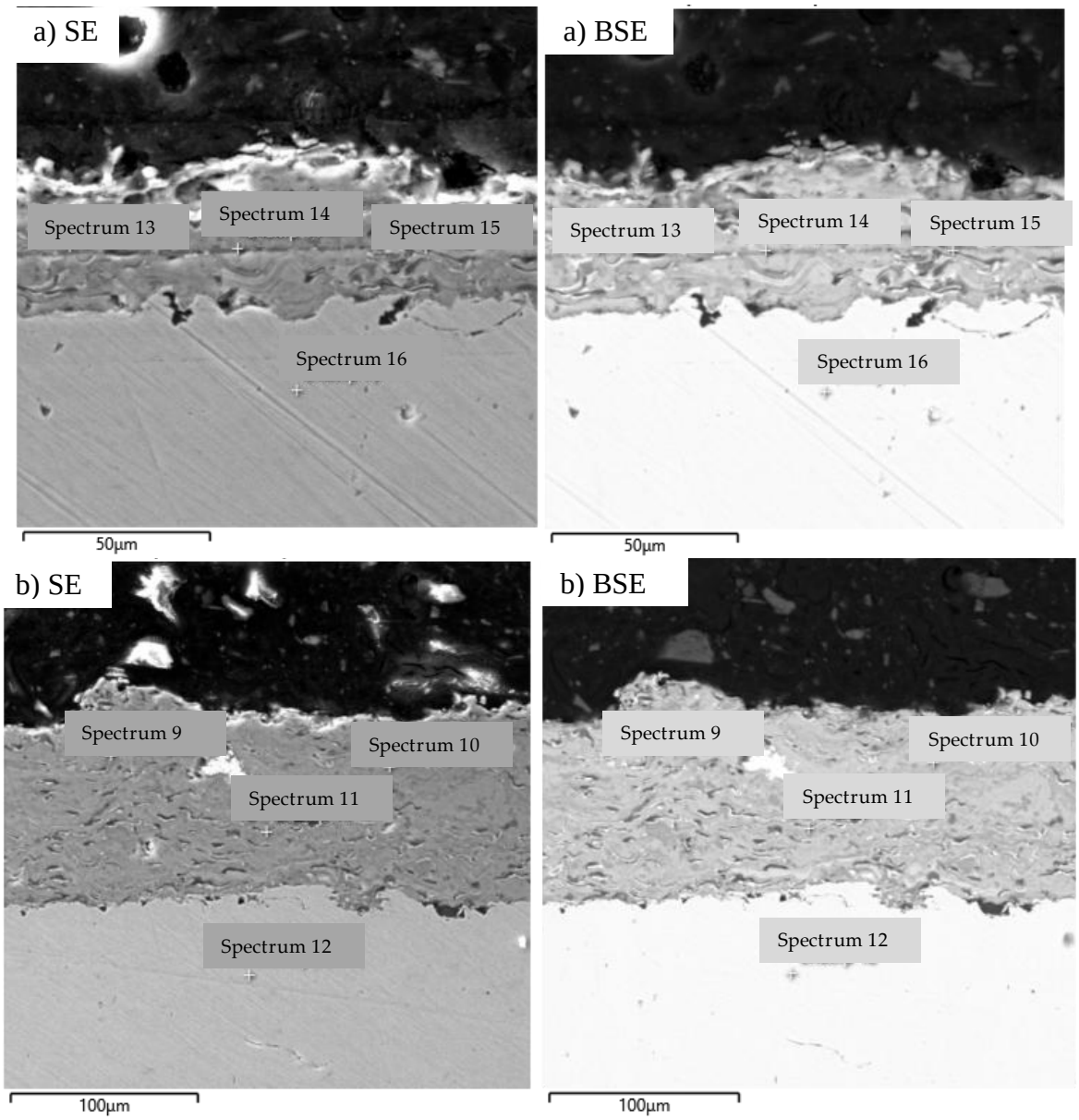

Figure 6. SE and BSE images in oxygen modes, sample: a) 3.0 bar b) 3.5 bar

To further evaluate the structural homogeneity of the coatings, a linear EDS analysis was performed on the cross-section of samples A (3.0 bar O_2) and B (3.5 bar O_2). The resulting element distribution profiles reveal phase formation features and the nature of the interface with the AISI 321 substrate.

Linear scanning shows that the main peaks correspond to Al (Kα ≈ 1.49 keV), Fe (Kα ≈ 6.40 keV), and Cu (Kα ≈ 8.04 keV), reflecting the basic composition of the Al-Cu-Fe system. However, the distribution profiles are characterized by pronounced intensity fluctuations, especially for Al and Cu, without the formation of clear plateaus within the layer. This indicates microstructural heterogeneity associated with incomplete melting of particles at reduced oxygen pressure [26]. Near the interface, a gradual increase in the Fe signal is observed, which may be due to both the contribution of the substrate and the formation of a transition zone involving Fe-Al intermetallic compounds [27]. The oxygen signal (O Kα ≈ 0.52 keV) is distributed unevenly, indicating the presence of local oxide inclusions along the interlamellar boundaries [28]. Overall, the profile indicates a less dense and more defective coating structure (Figure 7 and 8).

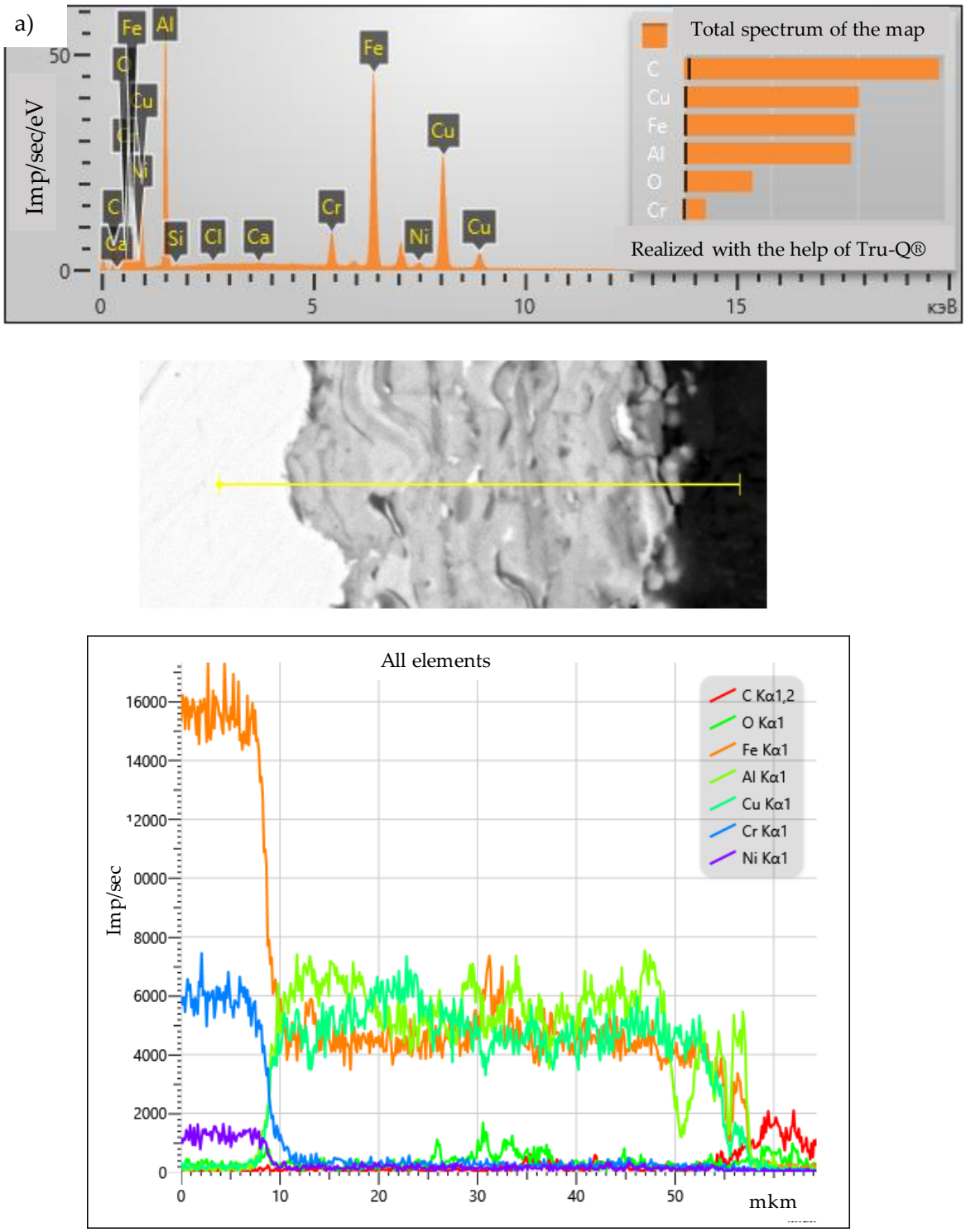

Figure 7. EDS analysis of sample A at 3.0 bar oxygen.

In this case, the Al, Cu, and Fe distribution profiles show distinct plateaus within the coating and a sharp drop in intensity at the interface with the substrate, indicating high chemical homogeneity of the la yer. The Cu distribution is uniform throughout the entire thickness, indicating the stability of the quasi-crystalline Al-Cu-Fe phase and the absence of segregation. The oxygen signal is moderate and relatively uniform, without pronounced local maxima, confirming limited oxidation under optimal thermal conditions. Near the interface, a clear Fe gradient is observed, caused by the transition to AISI 321 steel, with no signs of deep diffusion into the coating. This element distribution pattern indicates the formation of a dense, structurally intact layer with minimal porosity and a stable interphase boundary.

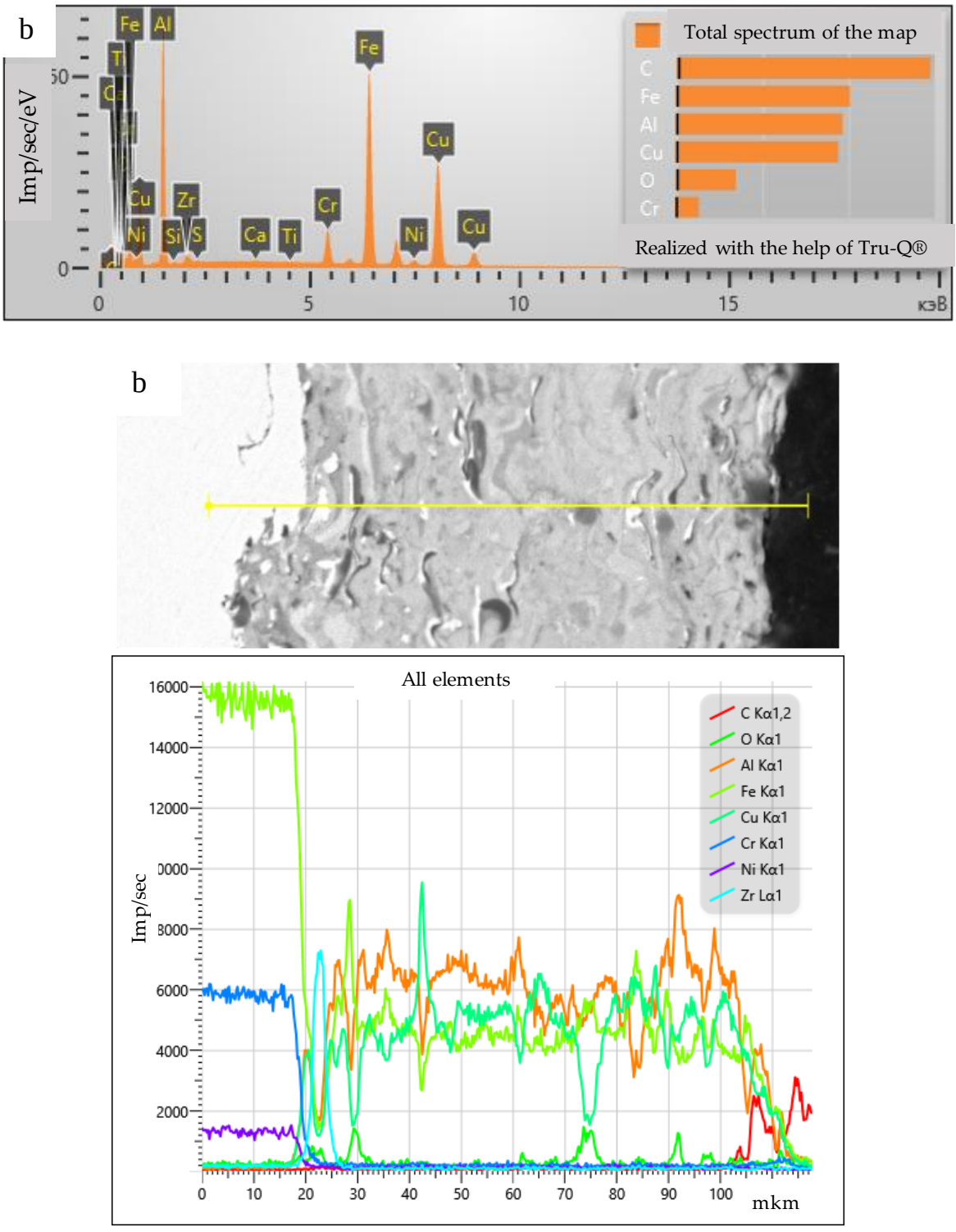

Figure 8. EDS analysis of sample A at 3.5 bar oxygen pressure

Thus, linear EDS analysis confirms that increasing the oxygen pressure to 3.5 bar promotes the formation of a more homogeneous and chemically stable microstructure compared to 3.0 bar, which correlates with the improved tribological properties of sample B.

4. Conclusion

Thus, the HVOF method successfully formed quasi-crystalline $Al_{65}Cu_{20}Fe_{15}$ coatings on an AISI 321 steel substrate with a thickness of 43.97 ± 3.0 μm at 3.0 bar oxygen pressure and 101.89 ± 13.5 μm at 3.5 bar. Coating formation was accompanied primarily by mechanical adhesion to the substrate without the formation of a

pronounced diffusion zone. X-ray diffraction analysis revealed the presence of the $Fe_{1.5}Al_{0.5}$ intermetallic phase and the quasi-crystalline phase of the Al-Cu-Fe system. With an increase in oxygen pressure to 3.5 bar, an increase in the proportion of the quasicrystalline component and a decrease in the relative intensity of the Fe-Al phase peaks are observed. SEM and EDS studies showed that at 3.5 bar, a denser and more chemically homogeneous structure with a minimal content of oxide inclusions is formed, whereas at 3.0 bar, microstructural heterogeneity and local porosity are observed. Tribological tests revealed that increasing the oxygen pressure from 3.0 to 3.5 bar leads to a decrease in the friction coefficient from 0.70-0.72 to 0.55-0.60 and a more than twofold reduction in the wear rate. The improved performance is associated with an increase in the proportion of the quasicrystalline phase and the formation of a stable tribofilm. Thus, an oxygen pressure of 3.5 bar is the optimal HVOF spraying mode for producing dense and wear-resistant $Al_{65}Cu_{20}Fe_{15}$ coatings on AISI 321 steel, designed for operation under conditions of intense friction and increased mechanical loads.

Funding: This research was funded by the Science Committee of the Ministry of Science and Higher Education of the Republic of Kazakhstan (grant no. AP26103943).

Acknowledgments: We express our gratitude to the Science Committee of the Ministry of Science and Higher Education of the Republic of Kazakhstan. For support of the project "Development of a composite ceramic-metal coating for protection against hydrogenation and high-temperature oxidation of zirconium alloy used in the nuclear industry".

References

1. Zhu L.; Soto-Medina S.; Cuadrado-Castillo W., et al. New Experimental Studies on the Phase Diagram of the Al–Cu–Fe Quasicrystal-Forming System. *Materials & Design*. **2020**, *vol.* 185, p. 108186.
2. Wolf W.; Koga G.Y.; Schulz R., et al. Wear and Corrosion Performance of Al–Cu–Fe–(Cr) Quasicrystalline Coatings Produced by HVOF. *Journal of Thermal Spray Technology*. **2020,** *vol.* 29, pp. 1195–1207.
3. Rahadilov B.K.; Kurbanbekov Sh.R.; Seitov B., et al. Teoreticheskie issledovaniya i optimizaciya rezhimov vysokoskorostnogo gazoplamennogo napyleniya pokrytij Cr_3C_2–NiCr. *Vestnik NYaC RK*. **2023**, no. 4, pp. 22–31.
4. Rahadilov B.K.; Muktanova N.; Kakimzhanov D.N. Vliyanie izmeneniya distancii napyleniya na strukturno-fazovoe sostoyanie i tribomekhanicheskie svojstva pokrytij 86WC–10Co–4Cr, poluchennyh metodom HVOF. *Vestnik NYaC RK*. **2024**, no. 3, pp. 91–104.
5. Panteleenko F.I.; Zhen P. Advanced Technologies of Laser Cladding and Thermal Spraying. *Litë i metallurgiya*. **2024**, no. 3, pp. 61–65.
6. Dubois J.M.; Belin-Ferré E. Friction and Solid–Solid Adhesion on Complex Metallic Alloys. *Science and Technology of Advanced Materials*. **2014**, *vol.* 15, no. 3, p. 034804.
7. Wang C.; Li Z.; Iefimov M.O., et al. Protection of AA2024 Alloy Against Wear and Corrosion by HVAF Sprayed AlCuFe Coating. *Surface Engineering*. **2023**, *vol.* 39, no. 5, pp. 532–540.
8. Kumar R.; Sharma S.; Singh J.P., et al. Enhancement in Wear Resistance of 30MnCrB5 Steel Using HVOF-Sprayed WC–10Co–4Cr Coatings. *Journal of Materials Research and Technology*. **2023**, *vol.* 27, pp. 1072–1096.
9. Mishra B.B.; Nautiyal H. Friction and Wear Behavior of Cr_3C_2–NiCr Coating on AISI 304 Stainless Steel. *Advances in Materials and Processing Technologies*. **2022**, *vol.* 8, no. 4, pp. 4007–4017.
10. Mora J.; García P.; Muelas R., et al. Hard Quasicrystalline Coatings Deposited by HVOF to Reduce Ice Accretion. *Coatings*. **2020**, *vol.* 10, no. 3, p. 290.
11. Shalaeva E.V.; Selyanin I.O.; Smirnova E.O., et al. Deformation Behavior of i-Al–Cu–Fe Quasicrystals Near Nanoindentation Imprint. *Physics of the Solid State*. **2018**, *vol.* 60, no. 2, pp. 307–314.
12. Huttunen-Saarivirta E.; Turunen E.; Kallio M. Microstructural Characterization of Thermally Sprayed Al–Co–Fe–Cr Coatings. *Journal of Alloys and Compounds*. **2003**, *vol.* 354, no. 1–2, pp. 269–280.
13. Wan P.; Cao D.H.; Zhou Y.J., et al. Impact of Annealing Treatment on the Properties of High-velocity Oxy-fuel Sprayed Al-Cu-Fe Quasi-crystalline Coating. *Surface Technology*. **2023**, *vol.* 52, no. 2, pp. 422–429.
14. ASTM G99-17. Standard Test Method for Wear Testing with a Pin-on-Disk Apparatus. West Conshohocken, PA: ASTM International, **2017**.
15. Rüdiger A.; Köster U. Corrosion Behavior of Al-Cu-Fe Quasicrystals. *Materials Science Forum*. **2000**, *vol*. 343–346, pp. 229–234.
16. Erkisi A.; Surucu G. First-Principles Study of DO_3-Type Fe_3M Alloys. *Politeknik Dergisi*. **2018**, *vol.* 21, no. 4, pp. 927–936.
17. Pougoum F.; Martinu L.; Klemberg-Sapieha J.E., et al. Wear Properties of Fe_3Al-Based HVOF Coatings. *Surface and Coatings Technology*. **2016**, *vol.* 307. Part A, pp. 109–117.

18. Babilas R.; Bajorek A.; Spilka M., et al. Structure and Corrosion Resistance of Al–Cu–Fe Alloys. *Progress in Natural Science: Materials International*. **2020**, *vol.* 30, no. 3, pp. 393–401.
19. Borisova A.L.; Borisov Yu.S.; Astakhov E.A., et al. Thermal Protection Properties of Quasicrystalline Coatings. *Avtomaticheskaya Svarka*. **2012**, no. 4, pp. 36–41.
20. Shalaeva E.V.; Prekul A.F. Structural Transformations in Al–Cu–Fe Quasicrystals. *Physics of Metals and Metallography.* **2010**, *vol.* 109, no. 4, pp. 424–433.
21. Fleury E.; Kim Y.C.; Kim J.S., et al. Sliding Wear of Quasicrystalline Coatings by HVOF. *Journal of Materials Research.* **2002**, *vol.* 17, no. 3, pp. 492–501.
22. Suárez M.A.; Esquivel R.; Alcántara J., et al. Effect of Composition on Al–Cu–Fe Alloys. *Materials Characterization*. **2011**, *vol*. 62, no. 10, pp. 917–923.
23. Kurbanbekov S.; Gaipov T.; Saidakhmetov P., et al. Microstructure and Tribological Properties of $Al_{65}Cu_{20}Fe_{15}$ Coatings Obtained by HVOF Method. *Lubricants*. **2025**, *vol.* 13, no. 7, p. 297.
24. Li L.; Bi Q.; Yang J., et al. Synthesis of Al–Cu–Fe Quasicrystals. *Scripta Materialia*. **2008**, *vol*. 59, no. 5, pp. 587–590.
25. Huttunen-Saarivirta E.; Turunen E.; Kallio M. Influence of Cr on Al–Cu–Fe Coatings. *Intermetallics*. **2003**, *vol*. 11, no. 8, pp. 879–891.
26. Torres A.; Serna S.; Patio C., et al. Corrosion Behavior of Ψ and β Quasicrystalline Al–Cu–Fe Alloy. *Journal of Materials Science and Engineering*. **2015**, *vol.* 5, no. 9–10, pp. 381–389.
27. Zhao H.Y.; Yang B.B.; Zhan J.F., et al. Study on the Electrochemical Impedance Spectroscopy of Strippable Coating on Different Metals. *Materials Protection*. **2018**, *vol.* 51, no. 9, pp. 45–48.
28. Study of the Structure, Physical and Chemical Properties of Al-Cu-Fe Quasicrystalline Materials. In *Proceedings of the Conference*; Frantsevich Institute for Problems of Materials Science: Kyiv, Ukraine, **2024**.